Noncollinear magnetism at interfaces in iron-chromium alloys: The ground states and finite-temperature configurations

M. Yu. Lavrentiev,[1] R. Soulairol,[2] Chu-Chun Fu,[2] D. Nguyen-Manh,[1] and S. L. Dudarev[1]
[1]*EURATOM/CCFE Fusion Association, Culham Centre for Fusion Energy, Abingdon, Oxfordshire OX14 3DB, United Kingdom*
[2]*CEA, DEN, Service de Recherches de Métallurgie Physique, F-91191 Gif-sur-Yvette, France*
(Received 4 August 2011; published 10 October 2011)

Noncollinear configurations of local magnetic moments at Fe/Cr interfaces in Fe-Cr alloys are explored using a combination of density functional theory (DFT) and magnetic cluster expansion (MCE) simulations. We show that magnetic frustration at Fe/Cr interfaces can be partially resolved through the formation of noncollinear magnetic structures, which occur not only at stepped but also at smooth interfaces, for example at the (110) interface where magnetic noncollinearity predicted by simulations is observed experimentally. Both DFT and MCE simulations predict that the magnetically frustrated (110) interface has the highest formation energy in the low-temperature limit. Using MCE and kinetic Monte Carlo simulations, we investigate the effect of temperature on magnetic order at interfaces and on interface energies. We find that while the low-temperature noncollinear bulk magnetic configurations of Cr remain stable up to the Néel temperature, the chromium atomic layers close to the interfaces retain their magnetic order well above this temperature. We also show that above the Curie temperature the (110) interface is the lowest energy interface, in agreement with DFT simulations of interfaces separating ferromagnetic Fe and nonmagnetic Cr.

DOI: 10.1103/PhysRevB.84.144203 PACS number(s): 75.50.Bb, 75.70.Cn, 64.70.kd, 64.75.Op

I. INTRODUCTION

Iron and chromium are 3*d*-transition metals characterized by complex structural and magnetic phase diagrams. Both adopt a body-centered cubic (bcc) crystal structure at low temperatures, where Fe is ferromagnetic (FM) and Cr is antiferromagnetic (AF), with local magnetic moments at the first-nearest-neighbor atom positions being antiparallel to each other. Recent *ab initio* investigations of FeCr alloys were carried out in the collinear magnetic approximation.[1–5] At the same time, there is compelling evidence that magnetic noncollinearity is fairly common in these alloys. For instance, experimental studies of iron-chromium interfaces[6–10] showed that thin Cr (100) and (110) films in contact with FM Fe have noncollinear magnetic structures where the local moments of Cr atoms are orthogonal to those of Fe atoms. These results were confirmed by self-consistent periodic Anderson model calculations performed for stepped (100) Fe/Cr interfaces.[11–13] Although the magnetic ground state of bulk Cr is best described as an incommensurate spin density wave (SDW),[14] both experimental and theoretical investigations of FeCr multilayers suggest that (100)-layered AF order is stable in the region close to the interface.[9,10,15,16] The occurrence of such AF order has been observed experimentally at temperatures up to 500 K, well above the Néel temperature of bulk Cr, for both the (100) and (110) Fe/Cr multilayers.[10,17]

Noncollinearity emerges as a way of resolving magnetic frustration, which stems from competing ferro- and antiferromagnetic interactions between the magnetic moments of Fe and Cr atoms. In the simplest model for Fe-Cr, both iron-chromium and chromium-chromium nearest-neighbor interactions are antiferromagnetic. This means that two Cr atoms surrounded by Fe atoms are magnetically frustrated, since the Fe-Cr interaction favors a magnetic configuration where Cr moments are parallel to each other and antiparallel to the Fe moments (here by "parallel" we mean "ferromagnetically ordered"), whereas the Cr-Cr interaction energy is minimum if the Cr moments are antiparallel. If there are only two chromium atoms present in the system, interaction with the iron environment is stronger than the Cr-Cr interaction, and in the resulting magnetic configuration the Cr moments end up being parallel to each other. However, as the number of Cr atoms increases, the outcome of competition between the Fe-Cr and Cr-Cr interactions becomes less obvious. In this case, the formation of a noncollinear configuration of magnetic moments provides the means for resolving magnetic frustration, as opposed to a collinear case where only abrupt changes in the orientation of magnetic moments, and consequently abrupt changes in magnetic energy, are possible.

Another fundamental deficiency of collinear magnetic models is their lack of dynamics. In a collinear magnetic system, an excitation corresponds to the reversal of the sign of a magnetic moment, resulting in a finite-size gap in the excitation energy spectrum. However, it is well known that elementary magnetic excitations (magnons) have a gapless spectrum, with the lowest energy excitations being long-wavelength spin waves.[18,19] In a classical Heisenberg model such waves can be described by small tilts of magnetic moments away from their equilibrium positions, which are impossible to realize in a purely collinear magnetic system. A dynamic noncollinear magnetic system evolves via atomic magnetic moments undergoing precession around their exchange vector fields.[20]

Recent simulations of chromium clusters in Fe-Cr alloys performed using the magnetic cluster expansion (MCE) model[21,22] showed that the local magnetic moments in the core of Cr clusters are not only noncollinear but are nearly *orthogonal* to the ferromagnetically ordered moments of Fe atoms and individual Cr atoms in the Fe-rich area of the alloy.[23] Independently, magnetic noncollinearity at (110) Fe/Cr interfaces was found in our density functional theory (DFT)

calculations performed using a bicrystal approximation.[24] These initial results prompted us to undertake a systematic study of magnetic noncollinearity in Fe-Cr alloys, and to investigate the fundamental origin of the phenomenon.

In this paper, we explore noncollinear magnetic configurations at Fe/Cr interfaces using a combined DFT and MCE approach. We show how magnetic noncollinearity helps resolve magnetic frustration inherent in a collinear model. We find that noncollinear magnetic structures form not only at stepped but also at smooth interfaces. Also, we investigate finite-temperature effects, both in terms of magnetic structures and interface energies, and explore how the magnetic properties of interfaces vary in the vicinity of magnetic phase transitions occurring in bulk Cr and Fe.

The paper is organized as follows. First, in Sec. II we derive magnetic equilibrium criteria for the classical Heisenberg-Landau Hamiltonian underpinning the magnetic cluster expansion model, and discuss implications of these criteria for the treatment of magnetic noncollinearity. Section III describes DFT investigations of Fe/Cr interfaces. In Sec. IV, we apply magnetic cluster expansion to the simulation of magnetic structures formed at interfaces, including the finite-temperature effects. The results are summarized in Sec. V.

II. MAGNETIC EQUILIBRIUM CONDITIONS

The magnetic cluster expansion model[21,22] uses a classical Heisenberg-Landau lattice Hamiltonian of the form[25]

$$\mathcal{H}(\mathbf{M}_1,\mathbf{M}_2,...,\mathbf{M}_N) = \sum_i A_i \mathbf{M}_i^2 + \sum_i B_i \mathbf{M}_i^4 + \sum_{i,j} J_{ij} \mathbf{M}_i \cdot \mathbf{M}_j, \quad (1)$$

where $\mathbf{M}_i$ is a magnetic moment associated with lattice site i, J_{ij} are the Heisenberg exchange parameters, and A_i and B_i are the Landau coefficients. At an extremum of this function, the terms linear in the infinitesimally small variations of magnetic moments $\delta\mathbf{M}_i$, $i = 1,2,...,N$, must vanish:

$$2A_i \mathbf{M}_i \cdot (\delta\mathbf{M}_i) + 4B_i \mathbf{M}_i^2 \mathbf{M}_i \cdot (\delta\mathbf{M}_i) + 2\sum_j J_{ij} \mathbf{M}_j \cdot (\delta\mathbf{M}_i) = 0. \quad (2)$$

Expressing each term $\delta\mathbf{M}_i$ as a sum of its magnitude and direction parts $\delta\mathbf{M}_i = \delta M_i \mathbf{e}_i + M_i \delta\mathbf{e}_i$, we can write condition (2) in the form

$$2A_i M_i \delta M_i + 4B_i M_i^3 \delta M_i + 2\sum_j J_{ij} M_j (\mathbf{e}_i \cdot \mathbf{e}_j)\delta M_i + 2\sum_j J_{ij} M_i M_j (\mathbf{e}_j \cdot \delta\mathbf{e}_i) = 0. \quad (3)$$

This equation shows that the magnitudes and orientations of magnetic moments $\mathbf{M}_i$ at equilibrium, which corresponds to a local minimum of function $\mathcal{H}(\mathbf{M}_1,\mathbf{M}_2,...,\mathbf{M}_N)$, are not independent quantities. It also shows that a magnetic configuration of an alloy, defined in terms of the magnitudes *and* directions of moments, depends on parameters A_i, B_i, and J_{ij}, which in turn depend sensitively on short- and long-range atomic order in the alloy.[21,22]

Writing $\delta\mathbf{e}_i$ as $\delta\mathbf{e}_i = \epsilon(\mathbf{e}_i \times \mathbf{n}_i)$, and in this way ensuring that $\delta\mathbf{e}_i \perp \mathbf{e}_i$, where $\mathbf{n}_i$ is an arbitrary vector and $\epsilon \ll 1$, we find a set of equations, the solution of which defines the *directions* of magnetic moments at equilibrium:

$$\sum_j J_{ij} M_i M_j [\mathbf{e}_j \cdot (\mathbf{n}_i \times \mathbf{e}_i)] = \sum_j J_{ij} M_i M_j [\mathbf{n}_i \cdot (\mathbf{e}_i \times \mathbf{e}_j)] = 0. \quad (4)$$

Given that the choice of vector $\mathbf{n}_i$ is arbitrary, we find that the extremum condition for the directions of magnetic moments is

$$\sum_j J_{ij} M_i M_j (\mathbf{e}_i \times \mathbf{e}_j) = \sum_j J_{ij} (\mathbf{M}_i \times \mathbf{M}_j) = \mathbf{M}_i \times \left(\sum_j J_{ij} \mathbf{M}_j \right) = 0. \quad (5)$$

This set of equations is equivalent to the condition [see Eq. (16) of Ref. 26] stating that the dynamic temperature of magnetic moments is zero. In terms of vector geometry, Eq. (5) states that at equilibrium each magnetic moment $\mathbf{M}_i$ is collinear with (but does not necessarily point in the same direction as) the exchange field $\sum_j J_{ij}\mathbf{M}_j$ acting on it. Numerical simulations carried out using realistic parametrizations of the MCE Heisenberg-Landau Hamiltonian[22] confirm that in all the cases explored in this work, including those involving complex magnetic noncollinearity, condition (5) is satisfied.

During the relaxation of electron degrees of freedom, the magnitudes and directions of magnetic moments evolve self-consistently toward equilibrium (3). The resulting configurations of magnetic moments may be collinear or noncollinear, depending on the sign, range, and magnitude of the Heisenberg exchange parameters J_{ij}. For example, condition (5) is obviously satisfied for any collinear configuration of magnetic moments, since the vector product of any two collinear vectors is zero.

However, the collinearity criterion (5) does not necessarily mean that the energy of a particular collinear configuration is minimum. For example, for a positive definite set of J_{ij} a collinear ferromagnetically ordered configuration of moments, although satisfying condition (5), corresponds to an energy maximum. This conclusion can be readily deduced from the examination of the original Heisenberg-Landau Hamiltonian (1), where the moment-orientation-dependent part of energy for a magnetic configuration, which is close to a ferromagnetic collinear configuration, has the form

$$\sum_{i,j} J_{ij} \mathbf{M}_i \cdot \mathbf{M}_j = \sum_{i,j} J_{ij} M_i M_j \left(1 - \Theta_{ij}^2/2 + \cdots\right), \quad (6)$$

where Θ_{ij} is the angle between vectors $\mathbf{M}_i$ and $\mathbf{M}_j$. This equation shows that for $J_{ij} > 0$ the exchange contribution to the total energy decreases as the angle Θ_{ij} between the two moments increases. Hence at an interface between two materials characterized by two different types of exchange interactions (favoring ferromagnetic *and* antiferromagnetic ordering of moments) it is natural to expect that the true energy minimum is realized for a complex noncollinear configuration of exchange

fields, and the corresponding noncollinear configuration of magnetic moments.

For the magnitude of magnetic moments, from Eq. (3) we find

$$A_i M_i + 2B_i M_i^3 + \sum_j J_{ij} M_j (\mathbf{e}_i \cdot \mathbf{e}_j) = 0, \tag{7}$$

which is equivalent to the condition

$$A_i M_i^2 + 2B_i M_i^4 + \mathbf{M}_i \cdot \left(\sum_{j \neq i} J_{ij} \mathbf{M}_j \right) = 0. \tag{8}$$

Comparing this with Eq. (5), we see that the magnitude M_i of magnetic moment at equilibrium satisfies the equation

$$A_i M_i^2 + 2B_i M_i^4 + \eta M_i \left| \sum_{j \neq i} J_{ij} \mathbf{M}_j \right| = 0, \tag{9}$$

where the choice of sign $\eta = \pm 1$ depends on whether the direction of moment $\mathbf{M}_i$ is the same as (+) or the opposite to (−) that of the local exchange field $\sum_j J_{ij} \mathbf{M}_j$. An energy minimum corresponds to $\eta = -1$ [in this case the Heisenberg exchange term $\mathbf{M}_i \cdot (\sum_j J_{ij} \mathbf{M}_j)$ in Hamiltonian (1) is negative]. The solution of Eq. (9) for $\eta = -1$ has the form

$$M_i = \sqrt{-\frac{A_i}{2B_i}} - \frac{1}{2A_i} \left| \sum_{j \neq i} J_{ij} \mathbf{M}_j \right| + \cdots. \tag{10}$$

This solution shows that the magnitude of magnetic moment $\mathbf{M}_i$ depends on the magnitude of the local exchange field acting on it. Hence the formation of noncollinear magnetic structures and the resulting variation of the local exchange fields necessarily gives rise to the variation in the magnitudes of magnetic moments. This occurs in addition to, and as a result of, the formation of a noncollinear magnetic configuration, where the orientations of magnetic moments are defined by the "zero magnetic temperature" condition (5).

In what follows we explore noncollinear magnetic configurations emerging as a result of interplay between complex exchange interactions between magnetic moments in FeCr alloys. The complexity of the problem stems from the fact that in pure Fe, exchange interactions favor ferromagnetic ordering of magnetic moments, whereas in pure Cr the moments order antiferromagnetically. We find that configurations of atomic magnetic moments at interfaces between iron and chromium, according to DFT and MCE simulations, are often strongly noncollinear in agreement with the analysis given above.

III. DENSITY FUNCTIONAL THEORY STUDY

A. Methodology

Ab initio calculations described below were performed using density functional theory implemented in the SIESTA code.[27] All the calculations are spin polarized, and they include the recent implementation of noncollinear magnetism.[28] Spin-orbit coupling effects are not considered. All the results presented in this paper were obtained using the generalized gradient approximation (GGA) exchange-correlation functional in the Perdew-Burke-Ernzerhof (PBE) form.[29]

With respect to other DFT approximations employed in this work, the core electrons are replaced by nonlocal norm-conserving pseudopotentials (NCPP), while the valence electrons are described by linear combinations of numerical pseudoatomic orbitals. The pseudopotentials and the basis sets for Cr and Fe are the same as in Refs. 30,31, where the accuracy of Cr and Fe pseudopotentials and basis sets was tested against the relevant known energy and magnetic properties. They were shown to agree with both the experimental data and accurate DFT values computed using projector augmented wave (PAW) pseudopotentials.[30]

Supercell calculations were performed for Fe-Cr interfaces. The bicrystal approximation was used, where each supercell contained two identical Fe/Cr interfaces, because of the constraint imposed by the three-dimensional periodic boundary conditions. In this study we only considered the perfectly coherent interfaces. Effects of steps and interdiffusion on magnetism are therefore beyond the scope of this paper. We considered various supercells, containing from 5 to 39 atomic layers of Cr and from 15 to 39 layers of Fe. The lateral dimensions of the cell were $a_0 \times a_0$, $\sqrt{2}a_0 \times a_0$, and $\sqrt{2}a_0 \times \sqrt{6}a_0$. These cells contained the (100), (110), and (111) interfaces, respectively, a_0 being the mean of the lattice parameters of bcc Fe and Cr. Calculations were performed assuming constant pressure conditions; i.e., the structures were optimized by relaxing both the atomic positions and the shape and volume of the supercell. In particular, all the residual stress components have been verified as being less than 5 kbar.

The k-point grids used for various supercells were adjusted according to the number of atoms in a cell. The grids were chosen to achieve k-space sampling equivalent to a cubic unit cell of bcc lattice with a $12 \times 12 \times 12$ shifted k grid. The Methfessel-Paxton broadening scheme with a 0.3 eV width was used. The calculated magnetic structures and interface formation energies were well converged with respect to the choice of k-point grids.

Complementary GGA calculations have also been carried out using more robust DFT implementations involving plane-wave basis sets. The results were used for validating the SIESTA values for some of the relevant cases. For validation, we used the PWSCF code,[32] which uses the ultrasoft pseudopotential (USPP), and the VASP code with projector augmented wave (PAW) potentials.[33–35] The kinetic-energy cutoffs for the plane-wave basis sets were 408 eV and 400 eV, respectively. The USPPs used for Fe and Cr are the same as in Ref. 30. We note that the same VASP-PAW approach was applied to parametrize the MCE Hamiltonian.[36,37]

B. Influence of magnetism on the energies of Fe/Cr interfaces

Our primary objective is the investigation of a possible connection between the energies and magnetic structures of Fe/Cr interfaces. For this purpose, we applied DFT to study interfaces between ferromagnetic bcc Fe and bcc Cr with various magnetic structures, namely the (100)-layered AF structure and a nonmagnetic (NM) structure. Noncollinear arrangements of magnetic moments in both Fe and Cr induced by the presence of interfaces have also been considered. In

TABLE I. Interface DFT formation energies (in J/m^2 units) between bcc Cr with various magnetic structures and FM Fe. The values from SIESTA are converged with respect to the number of Fe and Cr layers (m and n, respectively); i.e., $m,n = 39$ for the (100) and (111) interfaces, while $m,n = 15$ for the (110) case.

Cr Magnetic Order	AF	NM	NColl
(100)	0.11	0.14	0.17
(110)	0.19	0.09	0.17
(111)	0.13	0.12	0.19

what follows, the formation energy of an interface (E^f_{int}) is defined as

$$E^f_{\text{int}} = \frac{1}{2A}[E(\text{Cr}_n,\text{Fe}_m,2\,\text{int}) - E(\text{Cr}_n) - E(\text{Fe}_m)], \qquad (11)$$

where $E(\text{Cr}_n,\text{Fe}_m,2\,\text{int})$ denotes the total energy of a supercell containing n Cr layers and m Fe layers, and two identical interfaces. $E(\text{Cr}_n)$ and $E(\text{Fe}_m)$ are the total energies of the corresponding perfect bcc supercells containing the same number of n Cr and m Fe layers. The magnetic state of the reference Fe bulk system is always FM, whereas it may be either AF or NM for bulk Cr. In Eq. (11) A is the interface area, which is equal to a_0^2, $\sqrt{2}a_0^2$, and $\sqrt{12}a_0^2$ for the (100), (110), and (111) interfaces, respectively.

1. Collinear magnetic configurations

We start by considering interfaces between FM Fe and AF Cr, assuming a collinear arrangement of magnetic moments. The local magnetic structures of the three low-index interfaces, i.e., (110), (100), and (111), are schematically shown in the left panels of Figs. 1, 2, and 3, respectively. Since our goal is to understand properties of interfaces, it is important to consider a sufficient number of atomic layers so that the relevant computed values are fully converged. The converged formation energies for various interfaces are given in Table I. It is interesting to point out that we predict the lowest energy interface to be the (100), followed by the (111), and finally the (110). This trend, despite some quantitative discrepancies, is confirmed by the more robust plane-wave-DFT calculations, as shown in Table II. The energy ordering of interfaces found in DFT calculations is unexpected, given a simple "number of heterobonds" argument. Indeed, the general trend in bcc alloys exhibiting a tendency toward phase separation is that

TABLE II. Interface DFT formation energies (in J/m^2 units) between bcc Cr with various magnetic structures and FM Fe. The numbers of Fe and Cr layers, denoted by m and n, respectively, are equal to 15 for the AF and NM cases, while $m,n = 12$ for the noncollinear (NColl) structures. The SIESTA values are compared with the plane-wave-DFT ([a]PWSCF or [b]VASP) results, which are given in parentheses.

Cr Magnetic Order	AF	NM	NColl
(100)	0.11 (0.14[a])	0.14 (0.16[a])	0.17 (0.17[b])
(110)	0.19 (0.26[a])	0.09 (0.14[a])	0.17 (0.15[b])
(111)	0.13 (0.19[a])	0.12 (0.16[a])	0.20 (0.19[b])

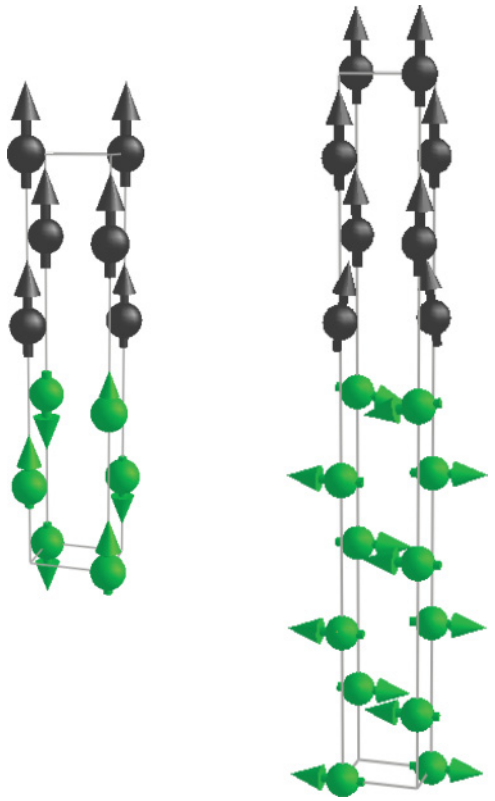

FIG. 1. (Color online) Schematic representation of the DFT magnetic structure of the (110) Fe/Cr interfaces with collinear (left) and noncollinear (right) magnetic order, showing Fe (black) and Cr (green) atoms near the interface. The magnitude and orientation of local magnetic moments are indicated by arrows.

the lower formation energies correspond to higher density interfaces; i.e., the (110) is expected to be the lowest energy interface. Our predictions are consistent with the earlier DFT data on adhesion energies of collinear (100) and (110) Fe/Cr interfaces.[2] On the other hand, the converged energies seem to differ from the calculations where very few Fe and Cr layers were considered and where residual interaction may still exist between the two interfaces in the same simulation cell. For instance, Lu *et al.*[3] found slightly higher interface energy for the (100) than for the (110) interface when considering relatively small supercells, i.e., those containing no more than 5 atomic layers of each element.

To understand the effect of magnetic ordering on such a reversal of relative interface stabilities, we first considered interfaces between FM Fe and NM Cr. At variance with the AF-Cr case, the lowest energy interface found in this case is indeed the (110), while the lower density (111) and (100) interfaces show higher formation energies. Note that the (111) interface is 0.02 J/m^2 lower in energy than the (100) according to the SIESTA results, while the PWSCF calculations suggest that the two interfaces are degenerate (see Table II).

The effect of magnetic ordering on interface formation energies may be explained by considering magnetic exchange coupling between Fe and Cr atoms near the interface (Figs. 1, 2, and 3). Based on bulk properties of bcc Fe and Cr, it is well known that FM order is preferable for Fe, where local moments of neighboring atoms have parallel orientations. On the other

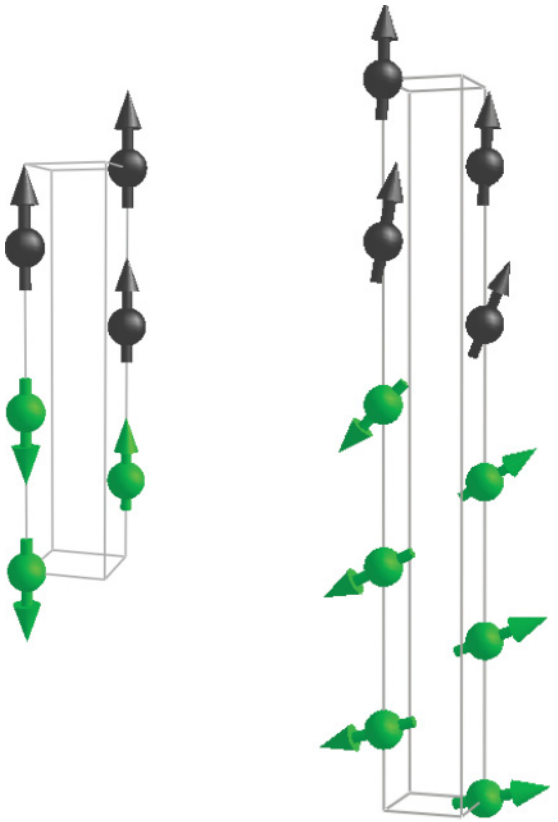

FIG. 2. (Color online) Schematic representation of the DFT magnetic structure of the (100) Fe/Cr interfaces with collinear (left) and noncollinear (right) magnetic order, showing Fe (black) and Cr (green) atoms near the interface. The magnitude and orientation of local magnetic moments are indicated by arrows.

hand, the first-nearest-neighbor (1*nn*) Cr moments tend to be antiparallel to each other. Also, earlier studies of FeCr alloys showed a tendency for the 1*nn* and 2*nn* Fe-Cr pairs to couple antiferromagnetically.[4,31]

Concerning the (110) interface (Fig. 1) where each atom has four and two intralayer 1*nn* and 2*nn* atoms respectively, we note clearly visible magnetic frustration at the interface associated with the parallel orientations of moments of the 1*nn*

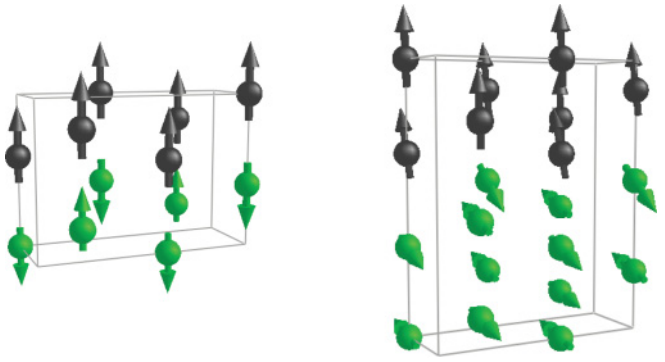

FIG. 3. (Color online) Schematic representation of the DFT magnetic structure of the (111) Fe/Cr interfaces with collinear (left) and noncollinear (right) magnetic order, showing Fe (black) and Cr (green) atoms near the interface. The magnitude and orientation of local magnetic moments are indicated by arrows.

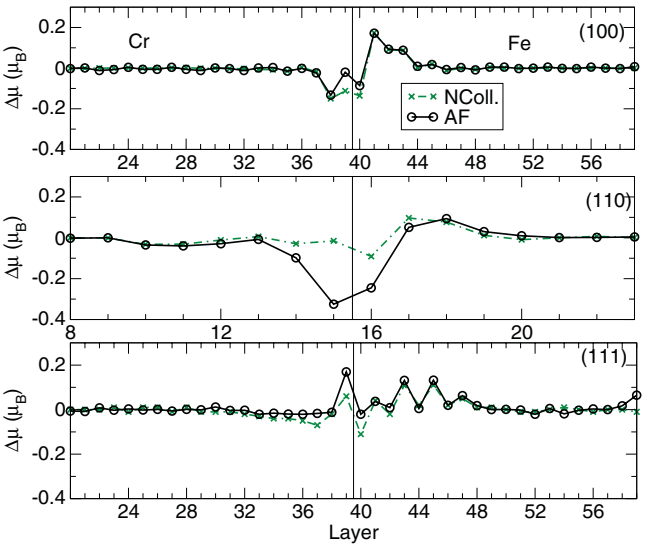

FIG. 4. (Color online) Variation of the magnitude of Cr and Fe DFT local moments (in μ_B) in the vicinity of the (100), (110), and (111) interfaces, in relation to their bulk values. Converged values are found for both collinear (Coll) and noncollinear (NColl) magnetic structures for the same supercells as those noted in Table I. For the (110) interfaces, only the values corresponding to Cr atoms situated in one of the two columns in the Fig. 1 are shown.

and 2*nn* Fe-Cr atomic pairs.[4] Magnetic frustration explains the significant increase of the (110) interface energy observed if magnetic order in Cr is switched from NM to AF.

In order to gain a more quantitative insight into the magnetic configurations associated with Fe/Cr interfaces, in Fig. 4 we show variation of Fe and Cr local moments ($\Delta\mu$) with respect to their bulk values. Note the decrease of magnitude of Cr and Fe moments, respectively, by $-0.33\ \mu_B$ and $-0.25\ \mu_B$ at the (110) interface, which is consistent with the effect in magnetic frustration mentioned above.

Regarding the (100) and (111) interfaces, we have only considered cases with odd numbers of Cr layers, so that Fe-Cr coupling across the interfaces within the supercell is antiparallel. There is therefore no magnetic frustration involving the first-nearest Fe-Cr neighbors, as for the (110) interface (Figs. 2, 3). However, when considering longer range Fe-Cr interactions, magnetic frustration still occurs because of the parallel magnetic orientation of moments at the interface Fe atoms and their second-nearest Cr neighbors.[4,31] Note that there are four 1*nn* Fe-Cr couplings per each interface Cr atom across both the (100) and the (111) interfaces, but the corresponding number of the 2*nn* couplings is different; i.e., there are three of them per atom for the Fe/Cr(111) and only one for the Fe/Cr(100) interface. This difference may influence the variation of the respective interface formation energies when switching from NM to AF Cr. Indeed, for the (100) case, the interface is strongly stabilized by the presence of four antiparallel 1*nn* Fe-Cr couplings per atom, whereas the influence of the parallel 2*nn* Fe-Cr pairs is relatively small. For the (111) case, however, the role played by the parallel 2*nn* Fe-Cr neighbors may be greater. The (111) interface energy therefore increases slightly if magnetic order in Cr is switched from NM to AF.

The effect of frustration is also illustrated by the local moment variation in the vicinity of interfaces, as shown in Fig. 4. For the (100) interface, we find that the local moment decreases slightly, by $-0.09\ \mu_B$ and $-0.14\ \mu_B$ for an interface Fe atom and a sub-interface Cr atoms, respectively. For the (111) interface, interestingly, no moment variation is found for the Cr atoms. Instead, we observe long-range oscillations of moments for the Fe atoms, before the magnetic moment solution converges to a bulk value.

2. *Noncollinear magnetic configurations*

Having discussed the effect of magnetic frustration on interface energies computed in the collinear magnetic moment approximation, we now attempt to find out whether it could act as a driving force for the formation of a noncollinear magnetic structure. Indeed, we find energy minima for the three low-index Fe/Cr interfaces, which correspond to noncollinear magnetic configurations. The corresponding interface formation energies are given in Table I.

At the (110) interface, magnetic frustration involving the 1*nn* and 2*nn* Fe and Cr atom pairs appears to represent the factor that induces noncollinear orientations of magnetic moments. The resulting lowest energy magnetic structure is shown in Fig. 1. Figure 5 shows the angle between the local moments of all the atoms and the FM ordered moments of Fe bulk atoms used as a reference. We note the pronounced overall *perpendicular* coupling between the Fe and Cr magnetic moments, which is in excellent agreement with experimental neutron diffraction measurements.[9,10] Only the moments of interface Fe and Cr atoms deviate slightly from the perfectly orthogonal order. This noncollinearity reduces the effect of Fe-Cr versus Cr-Cr frustration mentioned earlier in connection with collinear AF-Cr configurations. We see in Table I that the energy of the interface with a non-collinear configuration of magnetic moments is 0.02 J/m^2 lower than that corresponding to a constrained collinear AF-Cr configuration.

Also, the magnitude of moments on Fe and Cr atoms close to the interface increases significantly in comparison with the collinear case (Fig. 4), even though the moments are still smaller than their corresponding bulk magnitudes. Our results are consistent with the moment reduction observed by Mössbauer spectroscopy for the (110) interface.[38] Our findings also show that magnetic frustration associated with the collinearity constraint cannot be totally eliminated by removing this constraint.

Table III shows that noncollinear magnetic structures always have lower energy independently of the Cr-slab thickness. This is the case even for a very thin film of Cr, consisting of just five atomic layers. This explains why such magnetic structures have been observed experimentally for Fe/Cr (110) multilayers.[9,10] Besides the lowest energy configurations, we have also investigated other possible noncollinear energy minima, where the angle between the moments of the inner Cr atoms and the Fe moments varies from 0° and 90°. As a result, two other metastable states have been found, corresponding to angles of 20° and 45°. The interface energies are, respectively, 0.02 J/m^2 and 0.01 J/m^2 higher than those computed for the perpendicular magnetic configuration of the moments.

TABLE III. DFT formation energies (in J/m^2 units) of Fe/Cr (110) interfaces as a function of the number of Fe and Cr layers (m and n, respectively). Both collinear (Coll) and noncollinear (NColl) magnetic structures are included. For the collinear case, FM and AF configurations are considered for Fe and Cr, respectively.

m	15	15	15	29
n	5	13	15	29
Coll	0.19	0.18	0.19	0.19
NColl	0.18	0.17	0.17	

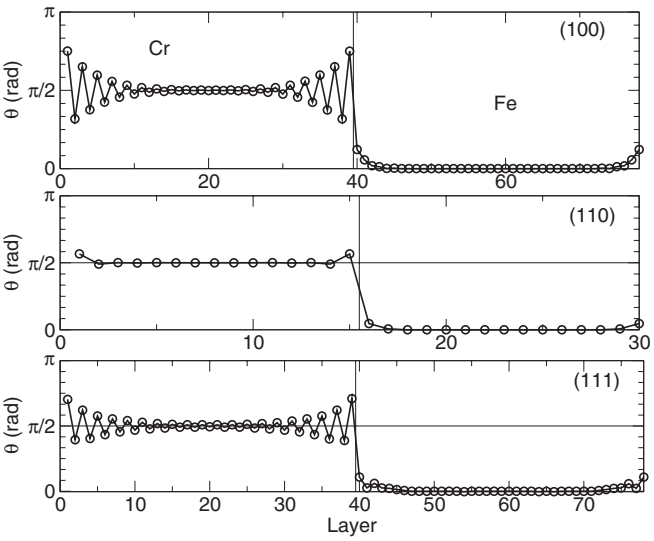

FIG. 5. Noncollinear DFT magnetic structures near Fe/Cr interfaces: absolute values of the angle between the local moments of various atoms and the moments of the inner bulklike Fe atoms. For the (110) interface, only the values corresponding to Cr atoms in one of the two columns in Fig. 1 are shown.

The situation is different for the (100) and (111) interfaces. The noncollinear magnetic structures are found to be unstable for thin films of Cr, and become metastable if the number of layers exceeds nine. Such structures show gradual variation of Cr moment directions, which are nearly collinear with the Fe moments at the interface and converge to a certain value of angle θ for the inner Cr layers. Several metastable solutions have been found for various $\theta > 0°$. The interface energy is maximum for $\theta = 90°$, and it decreases monotonically to a collinear configuration corresponding to $\theta = 0°$. Figures 2 and 3 give a schematic view of magnetic structures found for $\theta = 90°$. For comparison, the magnetic configuration of the (110) interface is shown in Fig. 1.

In contrast to the case of the (110) interface, there is no evidence that relaxation of magnetic frustration affects the magnitude of Cr moments (Fig. 4). Comparison of energies of collinear and noncollinear magnetic structures shows that the energy of the latter is higher by 0.06 J/m^2 for both the (100) and the (111) interfaces (Table I). Figure 5 clearly shows that, although such noncollinear structures may partly relax frustration associated with the parallel orientation of

moments for the 2*nn* Fe-Cr atoms, they also destroy the perfect antiparallel coupling between the four 1*nn* Fe-Cr moments at the interface. The resulting increase of the interface energy emerges as a result of the subtle balance between the two competing contributions, suggesting that the presence of the 2*nn* Fe-Cr magnetic frustration alone does not provide a strong enough driving force for stabilizing a noncollinear magnetic configuration.

Comparing all the interfaces between FM Fe and Cr with both collinear-AF and the noncollinear magnetic structures, we note that the (100) is the lowest energy interface among the three low-index interfaces. In the collinear magnetic case, the (110) is the highest energy interface. However, if the collinear constraint is removed, the energy of the (110) interface decreases slightly due to the partial relaxation of magnetic frustration (Table I).

IV. MAGNETIC CLUSTER EXPANSION STUDY

A. Magnetic cluster expansion model

The magnetic cluster expansion model was developed in Refs. 21,22 as a method that extends and generalizes the cluster expansion method[39,40] to the case of magnetic alloys. The MCE Hamiltonian explicitly treats both the configurational and magnetic degrees of freedom in alloys and is suitable for studying magnetic alloys such as Fe-Cr. The energy of an alloy configuration depends on both discrete site occupation variables σ_i ($\sigma_i = +1$ for Fe, $\sigma_i = -1$ for Cr), and the magnetic moments $\mathbf{M}_i$ of constituent atoms. The magnetic moment vectors have variable direction and magnitude. The MCE Hamiltonian is a sum of conventional cluster expansion terms and a Heisenberg-Landau magnetic part (1). The magnetic Heisenberg-Landau Hamiltonian depends explicitly on the underlying atomic configuration of the alloy via the Landau self-energy terms, which in a self-consistent way determine magnitudes of magnetic moments, and on the intersite Heisenberg magnetic interaction parameters. Atomic configurations and magnetic degrees of freedom are not independent, and hence the magnetic configuration of the alloy depends on its atomic configuration via the dependence of the Landau self-energy coefficients A_i, B_i and intersite Heisenberg exchange interaction parameters J_{ij} on the type of atomic species and their nearest-neighbor environment. At the same time, the energy of an atomic alloy configuration depends not only on the positions of atoms in the lattice, but also on the corresponding magnetic structure of the alloy.

In general, the MCE Hamiltonian includes atomic clusters of any size. In this work we use a MCE parametrization where only two-atom clusters are retained for both the nonmagnetic and magnetic terms:

$$\begin{aligned}\mathcal{H}(\{\sigma_i\},\{\mathbf{M}_i\}) &= N I^{(0)} + I^{(1)} \sum_i \sigma_i + \sum_{ij} I_{ij}^{(2)} \sigma_i \sigma_j \\ &+ \sum_i \left(A^{(0)} + A^{(1)} \sigma_i + \sigma_i \sum_j A_{ij}^{(2)} \sigma_j \right) \mathbf{M}_i^2 \\ &+ \sum_i \left(B^{(0)} + B^{(1)} \sigma_i + \sigma_i \sum_j B_{ij}^{(2)} \sigma_j \right) \mathbf{M}_i^4 \\ &+ \sum_{ij} \left(J_{ij}^{(0)} + J_{ij}^{(1)} (\sigma_i + \sigma_j) + J_{ij}^{(2)} \sigma_i \sigma_j \right) \mathbf{M}_i \cdot \mathbf{M}_j . \end{aligned} \quad (12)$$

Here N is the total number of atoms and $I^{(i)}$ are the nonmagnetic cluster expansion coefficients. Summation over i and j involves atoms occupying nearest-neighbor coordination shells. The functional form of Eq. (12) guarantees that the magnetic self-energy terms, and hence the directions and magnitudes of magnetic moments $\mathbf{M}_i$ predicted by the model, depend on the local environment of each atom in the alloy. Numerical values of parameters of Hamiltonian (12) for Fe-Cr alloys are given in Refs. 22,41. Note that Hamiltonian (12) does not include terms describing magnetic anisotropy effects and has no preferred direction in magnetic space, and hence is invariant with respect to a simultaneous rotation of all the magnetic moments $\mathbf{M}_i$ around an arbitrarily chosen axis by an arbitrary angle; such a transformation does not affect the energy of the system.

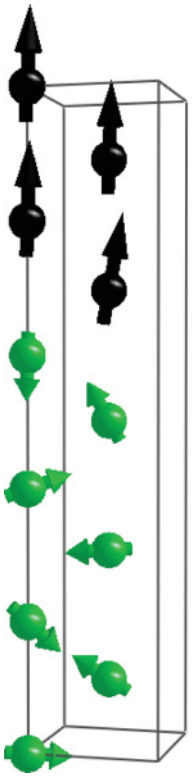

FIG. 6. (Color online) The MCE magnetic structure of the (100) Fe/Cr interface. Fe atoms are shown as black spheres, Cr atoms are green spheres.

B. Low-temperature magnetic structure of interfaces

We start by investigating low-temperature magnetic structures of the (100) Fe/Cr interface. Monte Carlo simulations are performed using a simulation cell containing 118 638 atoms ($39 \times 39 \times 39$ bcc unit cells) with periodic boundary conditions. The simulation cell is a bicrystal consisting of two slabs, Cr and Fe, each containing 39 atomic layers. At each

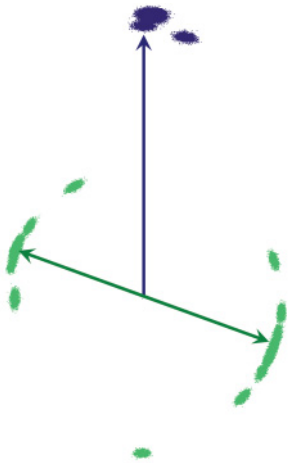

FIG. 7. (Color online) The MCE magnetic moments diagram for the (100) Fe/Cr interface. Fe moments are shown as dark-gray dots, Cr moments as green dots. Arrows represent directions of total magnetic moments for Fe and Cr subsystems.

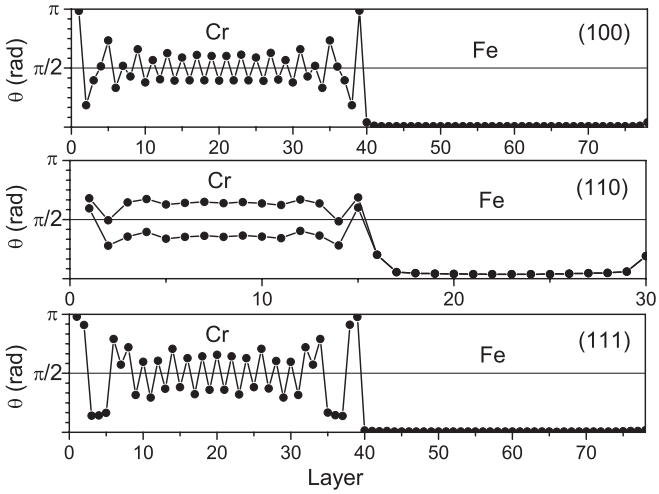

FIG. 8. Angle between the average Cr MCE magnetic moments in an atomic layer and the average Fe moment shown as a function of the number of the Cr layer. For the (110) Fe/Cr interface, two angles are shown for the Cr subsystem, corresponding to the two Cr columns with antiparallel (in the bulk) orientation of magnetic moments.

step, an attempt is made to change the magnetic moment of a randomly chosen atom. Both the direction and magnitude of vectors $\mathbf{M}_i$ are treated as variables. In this, as well as in all the other Monte Carlo simulations described in the paper, both the equilibration and accumulation stages of a simulation involve 8000 steps per atom.

The magnetic structure of the (100) Fe/Cr interface at low temperature ($T = 1$ K) is shown in Fig. 6. Four iron layers and seven chromium layers of atoms closest to the interface are shown. The magnetic moments are represented by arrows. One can immediately see that whereas Fe atoms retain parallel orientation of moments up to the interface, the Cr magnetic structure around the interface is different from that in the bulk. Similarly to the DFT results for the (100) Fe/Cr interface shown in the right panel of Fig. 2, while the atoms of the first chromium layer have their moments oriented almost exactly antiparallel to the nearest Fe atoms, further Cr atoms have their moments tilted farther and farther away from the Fe moments. Another visual illustration of magnetic structure of the (100) interface, the magnetic moments diagram, is given in Fig. 7. The vector of magnetic moment for each atom, characterized by its direction and magnitude, is shown here as a dot (assuming that the beginning of the vector corresponds to the origin of magnetic moment space), with different colors corresponding to different types of atoms (black for Fe and green for Cr, respectively). The resulting distribution of dots represents, in visual form, the distribution of directions and magnitudes (lengths) of magnetic moments for all the atoms in the alloy. The magnetic moment vectors lie almost in the same plane, which makes the two-dimensional representation shown Fig. 7 representative of the true three-dimensional distribution. Again, we see that the majority of the moments of chromium atoms are strongly tilted with respect to the FM ordered moments of the iron atoms.

To verify that the tilted rather than the orthogonal, configuration of Cr moments with respect to the Fe moments, corresponds to an energy minimum, we performed several Monte Carlo runs starting from various initial magnetic configurations. They included a random configuration, a collinear configuration, and a configuration where the initial Cr moments were assumed to be orthogonal to the FM ordered Fe moments. For all the configurations, the final magnetic structure diagrams were almost identical. The angles between the magnetic moments of Cr atoms in the middle of the chromium slab and the direction of Fe magnetization are 71°–73° and 106°–111° for consecutive layers of Cr. The total energies per atom for all the final configurations are within 0.001 meV of each other. We therefore conclude that the tilted orientation of chromium magnetic moments corresponds to the true ground state of the system described by the MCE Hamiltonian.

In order to visualize how the direction of Cr moments changes from being collinear to Fe moments at the interface to being tilted away from it, in Fig. 8 (top panel) we show the angle between the average Cr magnetic moments in various atomic layers, and the average Fe moment shown as a function of the number of atomic layer. The first (layer 1) and the last (layer 39) chromium layers are the interface layers in the direct proximity of iron atoms, and the Cr moments there are almost exactly collinear and antiferromagnetically aligned with respect to the iron moments. Farther away from the interface the moments deviate from collinearity. In the center of the Cr slab, chromium moments in the neighboring atomic layers are aligned antiferromagnetically with respect to each other, and tilted with respect to the Fe moments, so that the angle θ between the Cr and Fe moments is larger or smaller than $\pi/2$ in alternating chromium layers.

Simulations for the (110) Fe/Cr interface were performed using a cell containing 21 600 iron and 21 600 chromium atoms, with 15 atomic layers of each species (1440 atoms per layer). The magnetic structure in the region around the interface is shown in Fig. 9. Again, the transition from the ferromagnetic structure of Fe to the antiferromagnetic structure of Cr coincides with the change of the direction of magnetic moments. The difference from the (100) interface is that in

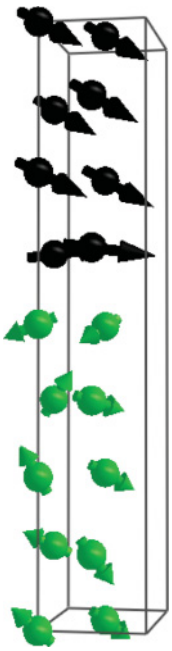

FIG. 9. (Color online) The MCE magnetic structure across the (110) Fe/Cr interface. Fe atoms are shown as black spheres, Cr atoms are green spheres.

the bulk of the Cr slab, each (110) layer includes atoms with antiparallel orientation of magnetic moments, corresponding to the two columns of Cr atoms in Fig. 9. Also, in the middle panel of Fig. 8 we show separately the angles between the average Fe moment and the Cr moment in each of the two chromium columns. As in to the (100) interface, the moments of bulk chromium atoms are not exactly orthogonal to those of the iron atoms, but are tilted with respect to the Fe moments so that the angle is $\sim 64^\circ$ in one column and $\sim 116^\circ$ in the other.

Finally, simulations of the (111) interface were performed for a system consisting of 6552 iron and 6552 chromium atoms (39 atomic layers for each subsystem), with the angle between the magnetic moments in the Cr and Fe region shown in the bottom panel of Fig. 8. The distance between the layers along the (111) axis is the smallest of the three interfaces studied here and, as a result, the transition region from the interface to the bulk magnetic structure of Cr involves more layers than in the case of either the (100) or (110) interfaces. The bulk behavior here is similar to the (100) case, with chromium moments in the adjacent layers aligned antiferromagnetically with respect to each other, and tilted with respect to the Fe moments (the angle between Cr and Fe moments is $\sim 65^\circ$ and $\sim 115^\circ$ in alternating Cr layers).

Thus the low-temperature magnetic structure for all three types of Fe/Cr interfaces follows a similar pattern. Starting from the chromium layers in contact with the iron subsystem, the direction of magnetic moments gradually deviates from collinearity, and in the bulk of the Cr slab the magnetic structure is antiferromagnetic, with the moments strongly tilted with respect to those of Fe. This behavior is driven by competition between various magnetic interactions, as discussed in Sec. IV E.

In MCE simulations, the lowest energy was found for the (111) interface, where it equals 0.23 J/m^2, as compared to 0.28 J/m^2 for the (100) and 0.35 J/m^2 for the (110) interfaces, respectively. These values are somewhat larger than the DFT values given in Sec. III. Energy ordering is different from that predicted by DFT, where the (100) interface is predicted to have lower energy than the (111). It is important to note that the (110) interface has a higher energy than the (100), in agreement with DFT.

Comparing the MCE and DFT results, we see that the behavior of magnetic moments for all three interfaces follows a similar pattern. There are differences; for example, in MCE the moments in the bulk of the Cr crystal are not exactly orthogonal to the iron moments, although they are strongly tilted with respect to the Fe moments. In DFT calculations, similar tilting takes place in several Cr layers near the interface, and then gives way to the orthogonal arrangement of moments in bulk Cr (Fig. 5). The occurrence of multiple metastable almost degenerate minima in DFT calculations, corresponding to various tilting angles of Cr moments (see Sec. III), suggests that there is no fundamental disagreement between the two approaches.

C. Temperature dependence of magnetic structure

As the temperature increases, magnetic moments of both Fe and Cr become disordered. For pure Cr, the transition from an antiferromagnetic to a paramagnetic state (occurring at the Néel temperature T_N) takes place at about 310 K.[19] MCE simulations of pure chromium predict a similar temperature of ~ 350 K.[41] While it is natural to expect that away from the Fe/Cr interface the temperature behavior of Cr is similar to that of the pure metal, at the interface the neighboring Fe layers may keep chromium moments in an ordered magnetic state even at temperatures higher than T_N. To verify this, we studied the temperature dependence of the magnetic properties of the (100) interface. We have chosen this interface because it is similar in terms of its magnetic properties to the (111) interface, and is simpler than the (110) interface where magnetic moments of Cr atoms in each layer are antiparallel. In Fig. 10 we show the dependence of the average magnitude of magnetic moments of Cr atoms on temperature and on the distance from the interface. For antiferromagnetic Cr, the direction of magnetic moment changes between layers, but within one layer all the magnetic moments point in the same direction. The average magnitude of magnetic moments in a given layer i, $|\langle \mathbf{M}_{\mathrm{Cr}}(i)\rangle|$, can thus serve as a measure of the degree of magnetic order in that layer, as it changes from $|\langle \mathbf{M}_{\mathrm{Cr}}(i)\rangle| \approx 1$ for completely antiferromagnetic Cr to $|\langle \mathbf{M}_{\mathrm{Cr}}(i)\rangle| \approx 0$ in paramagnetic chromium. Figure 10(a) confirms that several Cr layers, which are the closest to the interface, retain high magnetization even above the Néel temperature, at which the layers in the middle are already in a paramagnetic state. Note also that at the lowest temperature $T = 1$ K, the layers in direct contact with the Fe subsystem (layers 1 and 39) have magnetization higher than the rest of the chromium layers. At temperatures up to the Néel point, the magnetic structure of the Cr subsystem remains noncollinear. Above the Néel point, however, the moments with high magnetization are almost collinear to the moments of Fe. Figure 10(b) shows that while the inner layers of Cr have zero magnetization above 400 K, the two layers closest

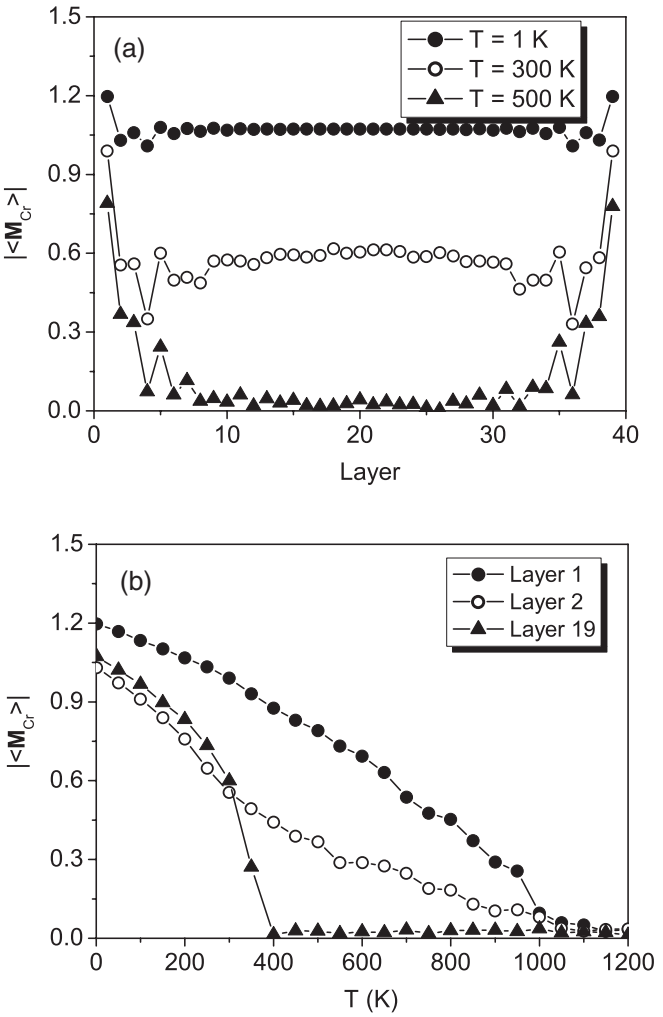

FIG. 10. Magnitude (in μ_B) of Cr magnetic moment shown as a function of atomic layer for the (100) Fe/Cr interface simulated using MCE for several temperatures (a), and the temperature dependence of the average MCE Cr magnetic moment near the Cr-Fe interface and in the bulk (b).

to the Fe-Cr interface retain nonzero magnetic moment almost up to the Curie temperature of Fe.

The effect of Cr on magnetic order in Fe atomic layers next to the (100) interface is illustrated in Fig. 11. We find that atomic layers of Fe closest to the interface exhibit the lowest magnetization. Also, these layers are the first to become paramagnetic as temperature increases, ahead of the bulk layers. This is in agreement with our simulations of the Curie transition in random Fe-Cr alloys.[41] We showed[41] that while at low concentrations the presence of Cr increases the Curie temperature when compared with pure iron, at concentrations above 10–15% Cr the Curie temperature is a decreasing function of Cr concentration. Hence we see that chromium at Fe/Cr interfaces suppresses ferromagnetism in atomic layers of iron close to the interface, whereas iron helps Cr maintain magnetic order near the interface at temperatures well above the Néel point.

The temperature dependence of interface energies for all three interfaces investigated in this work is shown in Fig. 12. We observe significant changes in energies in the vicinity of

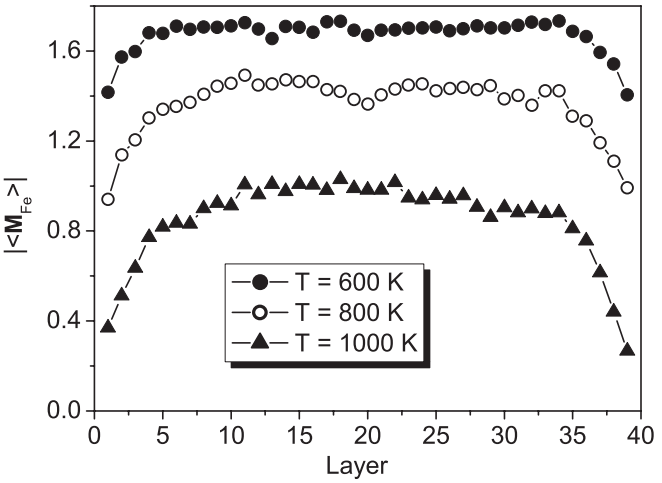

FIG. 11. Magnitude (in μ_B) of Fe magnetic moment vs atomic layer index at the (100) interface simulated using MCE for several temperatures.

magnetic phase transitions occurring in both Cr and Fe. The Néel transition in chromium and the Curie transition in iron give rise to a substantial reduction of formation energies for all three interfaces. The (110) interface energy exhibits the largest fall above the Néel point and at higher temperatures closer to the Curie point, resulting in a change in the order of interface energies, with the (110) interface becoming the lowest energy interface for $T > 900$ K. This correlates with results of Sec. III B, where the lowest energy interface is of the (110) type, provided that it separates FM Fe and NM Cr. We believe that magnetic frustration at the interface resulting from ferromagnetic coupling between one half of the nearest Fe-Cr neighbors, mentioned in Sec. III B, persists at high temperatures, and vanishes only after magnetization in the first interfacial Cr layer reduces to zero [see Fig. 10(b)]. After that, the (110) becomes the lowest energy interface, in agreement with results given in Table I.

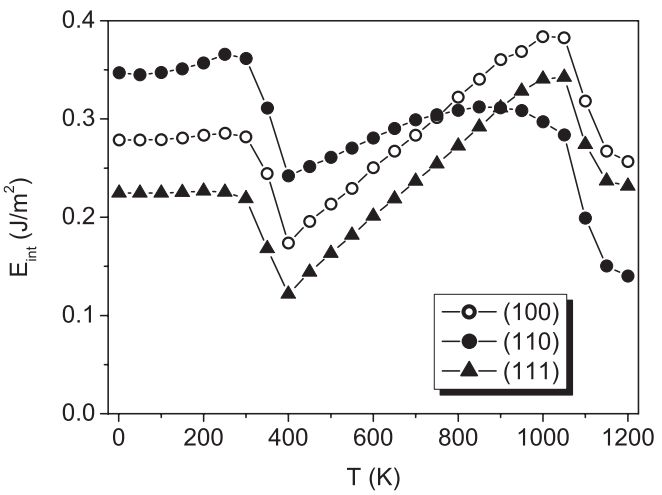

FIG. 12. Temperature dependence of the MCE interface formation energies.

D. Interfaces involving Fe-Cr solid solutions

Recent experimental and theoretical studies of the Fe-Cr phase diagram[42] and the observed inversion of short-range order[43] show that Cr is soluble in Fe even at low temperatures. This justifies simulations of interfaces between pure Cr and solid solutions of Cr in the Fe matrix. Using MCE, we simulated the magnetic structure and energy for the (100) interface between pure Cr and random alloy $Fe_{0.9}Cr_{0.1}$. The interface energy was found to be 0.07 J/m^2, which is almost four times lower than the energy of the (100) Cr-Fe interface (Sec. IV B). Magnitudes of magnetic moments of Cr atoms dissolved in iron are larger than those of bulk chromium (1.33–1.35 μ_B vs 1.05–1.1 μ_B). Cr atoms at the first (interface) layer of Fe also have smaller magnetic moments similar to the moment of bulk Cr. On the chromium side of the interface, moments of atoms are smaller than at the interface of Cr with pure Fe (1.13 μ_B vs 1.20 μ_B in the interface Cr layer). This could be one of the reasons for the decrease of the interfacial energy. Directions of moments for all the chromium atoms in the solution are antiparallel to those of pure Fe.

Inserting an iron atom into pure chromium does not result in a noticeable change of magnetic structure of the nearby Cr atoms. At the same time, the direction of the magnetic moment of a Fe atom near a (100) interface depends strongly on the distance between the atom and the interface. In the interface chromium layer, the moment of the embedded Fe atom is parallel to the moments of bulk iron atoms, whereas the same atom embedded in the third Cr layer exhibits antiparallel orientation of the moment. If the atom is embedded in an even (the second or the fourth) Cr layer, its moment is nearly orthogonal to that of bulk Fe. Far away from the interface the direction of the moment of the embedded Fe atom is determined by the surrounding Cr atoms only.

E. Emergence of noncollinearity in a simplified model for a Fe/Cr interface

Rotation of magnetic moments at the interface observed in our simulations represents a way of resolving magnetic frustration. Consider for example the (100) Fe/Cr interface with nearest-neighbor magnetic interactions favoring AF Fe-Cr and Cr-Cr moments alignment. If only those interactions were effective, the interface Cr layer would have an opposite moment to that of iron; the second Cr layer would have its moment opposite to those of the first Cr layer, etc. In this case, FM Fe and AF Cr structure would coexist at the interface. However, if the range of magnetic interactions extends further, the system becomes frustrated. The tendency of magnetic moments to align noncollinearly across the interface in this case can be understood if both the second-nearest-neighbor Fe-Cr and Cr-Cr interactions were antiferromagnetic. Then, the second chromium layer would tend to align antiferromagnetically with respect to both Fe and the first Cr layer; as this is impossible, some adjustment of the direction of moments in both layers is necessary to reduce energy. Moments in the third Cr layer would then tend to align antiferromagnetically with respect to the first two, which is also impossible, resulting in the further change of the direction of moments.

The following simplified MCE Hamiltonian model may help understand the instability of collinear magnetic order and explain the emergence of noncollinearity at the (100) Fe/Cr interface. Let us assume that all the Fe moments are aligned ferromagnetically everywhere, including at the interface. We further assume that the magnitudes of Cr and Fe moments do not vary (they are 2.23 μ_B for iron and 1 μ_B for chromium, respectively) and that only the first- and second-nearest-neighbor Heisenberg interactions are significant. In this case, the relevant terms of the MCE Hamiltonian (12) are

$$E = \sum_{i\in \mathrm{Fe},\, j\in \mathrm{Cr}} J_{ij}^{\mathrm{Fe\text{-}Cr}} \mathbf{M}_i \cdot \mathbf{M}_j + \sum_{i,\, j\in \mathrm{Cr}} J_{ij}^{\mathrm{Cr\text{-}Cr}} \mathbf{M}_i \cdot \mathbf{M}_j. \quad (13)$$

All four interaction terms ($J_{ij}^{\mathrm{Fe\text{-}Cr}}$ and $J_{ij}^{\mathrm{Cr\text{-}Cr}}$ for the first- and second-nearest neighbors, respectively) are positive in (13), favoring AF alignment of moments. This is in agreement with our parametrization of the MCE Hamiltonian,[22,41] as well as with the phenomenological model proposed by Klaver *et al.*[4]

If both the second-nearest-neighbor coefficients are equal to zero, the ground state of the system is AF collinear with the first (interfacial) Cr layer having antiparallel magnetic ordering with respect to Fe moments. The angle θ_i between magnetization of iron and magnetization of chromium in layer i is then equal to π for odd and zero for even layers, respectively. This ground state corresponds to an energy minimum with respect to small changes of θ_i. Increasing the second-nearest-neighbor Heisenberg coefficients results in the loss of stability of this minimum at some critical value of $J_{ij}^{\mathrm{Fe\text{-}Cr}}(2nn)$ and $J_{ij}^{\mathrm{Cr\text{-}Cr}}(2nn)$ in accordance with the criteria described above. At this critical point, the collinear ground state becomes unstable with respect to small changes of θ_i. The onset of this instability can be detected by examining the eigenvalues of the matrix of second derivatives of energy with respect to θ_i. We investigated the limits of stability of the ground state as a function of $J_{ij}^{\mathrm{Fe\text{-}Cr}}(2nn)$ and $J_{ij}^{\mathrm{Cr\text{-}Cr}}(2nn)$ assuming that the nearest-neighbor Heisenberg coefficients are given by the current parametrization of the MCE model [$J_{ij}^{\mathrm{Fe\text{-}Cr}}(1nn) = 19.881$ meV, $J_{ij}^{\mathrm{Cr\text{-}Cr}}(1nn) = 5.555$ meV]. Calculations were performed for a large system containing over 40 chromium layers. Figure 13 shows a region in the parameter space where the collinear antiferromagnetic structure retains its stability. Another possible collinear ground state structure can form if the second-nearest-neighbor coefficient $J_{ij}^{\mathrm{Fe\text{-}Cr}}(2nn)$ is sufficiently large. In this case, both the first and the second interfacial layers of Cr are ordered antiferromagnetically with respect to iron, and alternating chromium layers begin with layer 3. This collinear state exists for large $J_{ij}^{\mathrm{Fe\text{-}Cr}}(2nn)$ and small $J_{ij}^{\mathrm{Cr\text{-}Cr}}(2nn)$, and its region of stability is also shown in Fig. 13. The actual values of the second-nearest-neighbor interaction coefficients are shown in Fig. 13 by the star symbol. They are in the region where both collinear ground states are unstable, resulting in the system adopting a noncollinear magnetic ground state.

Of course, this consideration is rather simplified, and it does not take into account interactions that extend farther than the second-nearest-neighbor distance. It is also possible that there are other collinear magnetic structures stable in some other regions of the parameter space. Still, the model confirms that the reason for the formation of a noncollinear magnetic configuration are the nonzero second-nearest-neighbor magnetic interactions, showing how the most obvious collinear

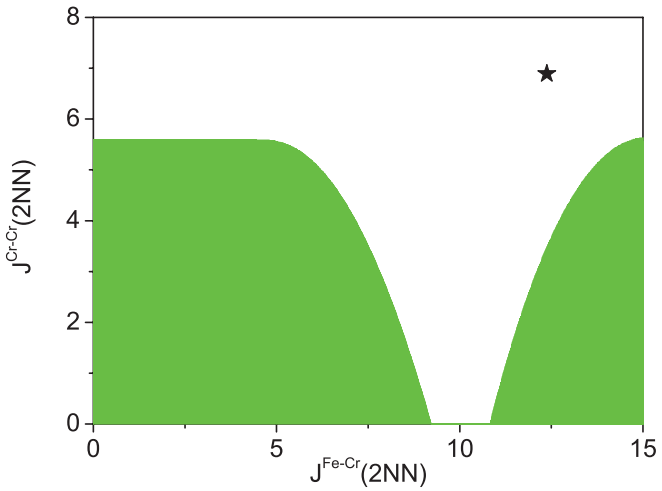

FIG. 13. (Color online) Regions in the space of the second-nearest-neighbor interaction parameters where the collinear magnetic structure at the (100) Fe/Cr interface is stable (shaded). The star sign indicates the actual values of these parameters in the MCE model.

ground states lose stability if $J_{ij}^{\text{Fe-Cr}}(2nn)$ and $J_{ij}^{\text{Cr-Cr}}(2nn)$ become large in comparison with the first-nearest-neighbor interactions. This model can be readily extended to investigate the stability of collinear structures without the need to resort to time-consuming Monte Carlo simulations. The model shows that even small changes in magnetic interactions, including long-range interactions, may result in the destabilization of the global magnetic ground state. This may explain the difference between DFT and MCE results for the (100) and (111) interfaces described earlier in this paper.

Regarding the (110) interface, as was noted in Sec. III B, there is additional magnetic frustration resulting from the nearest-neighbor AF interaction between Cr atoms in the same layer. This additional frustration may explain the fast convergence of the noncollinear magnetic structure, as compared to the (100) and (111) interfaces, shown in Fig. 5.

V. CONCLUSIONS

We have performed a combined *ab initio* and MCE Monte Carlo investigation of three low-index Fe/Cr interfaces, the (100), the (110), and the (111), and explored interface energies and magnetic structures formed at zero and finite temperatures. We found that magnetic noncollinearity characterizes even smooth Fe/Cr interfaces.

Density functional theory calculations were applied to investigate the anisotropy of interface energies at three Fe/Cr interfaces as a function of Cr magnetic configuration, including the collinear AF- and NM-Cr as well as noncollinear magnetic structures. Contrary to what was expected for an interface between two bcc metals exhibiting phase separation, the (110) interface has the highest energy among the three interfaces in the presence of magnetism. This is a direct consequence of magnetic frustration resulting from competing bulk FM-Fe and AF-Cr magnetic ordering effects and antiferromagnetic Fe-Cr 1*nn* and 2*nn* coupling at the interface. Once the collinear constraint is removed, the energy of the interface decreases due to partial relaxation of magnetic frustration. On the other hand, all the noncollinear structures are found to be metastable and higher in energy than the respective collinear configurations for the (100) and (111) interfaces. This comes from a subtle balance between two competing interactions. On the one hand, the Fe-Cr 1*nn* antiparallel coupling at the interface is best satisfied in a collinear structure. On the other hand, in a noncollinear structure, magnetic frustration associated with the parallel orientation of moments for the 2*nn* Fe-Cr atoms is partially relaxed, but at the same time this also destroys the perfect antiparallel coupling between the 1*nn* Fe-Cr moments.

Both collinear and noncollinear magnetic structures for the low-energy states are investigated in detail. In particular, the reduction of magnitudes of local moments near the interface has been shown to represent a visible signature of magnetic frustration. We also note that the lowest energy magnetic configuration of the (110) interface is such that the local moments of bulk Fe and Cr atoms are orthogonal to each other, in excellent agreement with the available experimental data.

MCE simulations showed that at large distances from all the three interfaces, the moments of Cr atoms in the lowest energy configuration are noncollinear with respect to those of Fe atoms. The general trends exhibited by magnetic structures follow a pattern similar to that predicted by DFT. At large distances from the interface, we find that magnetic moments of Cr atoms are tilted with respect to, but not exactly orthogonal to, those of iron atoms. The (110) interface was found to have the largest interface energy of the three Fe/Cr interfaces at low temperature, in agreement with DFT calculations for magnetic Cr.

The temperature variation of magnetic structures near the interfaces was investigated using the MCE model and large-scale Monte Carlo simulations. Noncollinear configurations found at low temperatures remain stable up to the Néel temperature. The interface energy exhibits significant variation near the magnetic phase transition temperatures. Magnetization of interface layers of Cr remains nonzero at temperatures well above the Néel temperature, due to exchange interactions between Cr and Fe moments. At the same time, interaction with chromium across the interface suppresses ferromagnetism in iron. At temperatures close to the Curie point the (110) interface has the lowest energy, in agreement with DFT calculations for the FM Fe - NM Cr interface.

ACKNOWLEDGMENTS

We acknowledge support from a travel grant provided to CCFE, CEA, and the University of Oxford by the French Embassy in the UK, and support from the EURATOM staff mobility program. This work was partly funded by the European Communities under the Contracts of Association between EURATOM and CCFE, and EURATOM and CEA, and was carried out within the framework of European Fusion Development Agreement. The views and opinions expressed herein do not necessarily reflect those of the European Commission. Work at CCFE was partially funded by the RCUK Energy Programme under Grant No. EP/I501045. We also acknowledge the use of HPC resources provided by GENCI-CINES (Grant No. 2011-x2011096020) and the use of HPC for Fusion Facilities at Jülich.

[1]P. Olsson, C. Domain, and J. Wallenius, Phys. Rev. B **75**, 014110 (2007).
[2]D. F. Johnson, D. E. Jiang, and Emily A. Carter, Scr. Metall. Mater. **601**, 699 (2007).
[3]S. Lu, Q.-M. Hu, R. Yang, B. Johansson, and L. Vitos, Phys. Rev. B **82**, 195103 (2010).
[4]T. P. C. Klaver, R. Drautz, and M. W. Finnis, Phys. Rev. B **74**, 094435 (2006).
[5]K. O. E. Henriksson, J. Nucl. Mater. **395**, 45 (2009).
[6]P. Bödeker, A. Hucht, A. Schreyer, J. Borchers, F. Güthoff, and H. Zabel, Phys. Rev. Lett. **81**, 914 (1998).
[7]P. Bödeker, A. Schreyer, and H. Zabel, Phys. Rev. B **59**, 9408 (1999).
[8]H. Zabel, J. Phys. Condens. Matter **11**, 9303 (1999).
[9]H. Fritzsche, J. Hauschild, A. Hoser, S. Bonn, and J. Klenke, Europhys. Lett. **49**, 507 (2000).
[10]H. Fritzsche, S. Bonn, J. Hauschild, J. Klenke, K. Prokes, and G. J. McIntyre, Phys. Rev. B **65**, 144408 (2002).
[11]V. M. Uzdin, N. S. Yartseva, and S. V. Yartsev, J. Magn. Magn. Mater. **196-197**, 70 (1999).
[12]V. M. Uzdin, A. Mokrani, C. Demangeat, and N. S. Yartseva, J. Magn. Magn. Mater. **198-199**, 471 (1999).
[13]N. S. Yartseva, S. V. Yartsev, V. M. Uzdin, and C. Demangeat, Comput. Mater. Sci. **17**, 468 (1999).
[14]E. Fawcett, Rev. Mod. Phy. **60**, 209 (1988).
[15]K. Hirai, Phys. Rev. B **59**, R6612 (1999).
[16]R. Fishman, J. Phys. Condens. Matter **13**, R235 (2001).
[17]A. Schreyer, C. F. Majkrzak, Th. Zeidler, T. Schmitte, P. Bödeker, K. Theis-Bröhl, A. Abromeit, J. A. Dura, and T. Watanabe, Phys. Rev. Lett. **79**, 4914 (1997).
[18]R. P. Feynman, *Statistical Mechanics* (Benjamin, Reading, MA, 1972).
[19]S. Blundell, *Magnetism in Condensed Matter* (Oxford University Press, Oxford, 2001).
[20]P.-W. Ma, C. H. Woo, and S. L. Dudarev, Phys. Rev. B **78**, 024434 (2008); P.-W. Ma and C. H. Woo, Phys. Rev. E **79**, 046703 (2009); P.-W. Ma and S. L. Dudarev, Phys. Rev. B **83**, 134418 (2011).
[21]M. Yu. Lavrentiev, S. L. Dudarev, and D. Nguyen-Manh, J. Nucl. Mater. **386–388**, 22 (2009).
[22]M. Yu. Lavrentiev, D. Nguyen-Manh, and S. L. Dudarev, Phys. Rev. B **81**, 184202 (2010).
[23]M. Yu. Lavrentiev, D. Nguyen-Manh, and S. L. Dudarev, Solid State Phenomena **172–174**, 1002 (2011).
[24]R. Soulairol, Chu-Chun Fu, and C. Barreteau, Phys. Rev. B **84**, 155402 (2011).
[25]S. L. Dudarev and P. M. Derlet, J. Comput.-Aided Mater. Design **14**, 129 (2007).
[26]P.-W. Ma, S. L. Dudarev, A. A. Semenov, and C. H. Woo, Phys. Rev. E **82**, 031111 (2010).
[27]J. Soler, E. Artacho, J. Gale, A. Garcia, J. Junquera, P. Ordejón, and D. Sanchez-Portal, J. Phys. Condens. Matter **14**, 2745 (2002).
[28]V. M. García-Suárez, C. M. Newman, C. J. Lambert, J. M. Pruneda, and J. Ferrer, J. Phys. Condens. Matter **16**, 5453 (2004).
[29]J. P. Perdew, K. Burke, and M. Ernzerhof, Phys. Rev. Lett. **77**, 3865 (1996).
[30]R. Soulairol, Chu-Chun Fu, and C. Barreteau, J. Phys. Condens. Matter **22**, 295502 (2010).
[31]R. Soulairol, Chu-Chun Fu, and C. Barreteau, Phys. Rev. B **83**, 214103 (2011).
[32]See [http://www.pwscf.org/].
[33]G. Kresse and J. Hafner, Phys. Rev. B **47**, 558 (1993).
[34]G. Kresse and J. Furthmüller, Phys. Rev. B **54**, 11169 (1996).
[35]G. Kresse and D. Joubert, Phys. Rev. B **59**, 1758 (1999).
[36]D. Nguyen-Manh, M. Yu. Lavrentiev, and S. L. Dudarev, J. Comput.-Aided Mater. Design **14**, 159 (2007).
[37]D. Nguyen-Manh, M. Yu. Lavrentiev, and S. L. Dudarev, C. R. Phys. **9**, 379 (2008).
[38]N. Jiko, M. Almokhtar, K. Mibu, and T. Shinjo, J. Phys. Condens. Matter **17**, 2477 (2005).
[39]J. M. Sanchez, F. Ducastelle, and D. Gratias, Physica A **128**, 334 (1984).
[40]M. Yu. Lavrentiev, R. Drautz, D. Nguyen-Manh, T. P. C. Klaver, and S. L. Dudarev, Phys. Rev. B **75**, 014208 (2007).
[41]M. Yu. Lavrentiev, D. Nguyen-Manh, and S. L. Dudarev, Comput. Mater. Sci. **49**, S199 (2010).
[42]W. Xiong, M. Selleby, Q. Chen, J. Odqvist, and Y. Du, Crit. Rev. Solid State Mater. Sci. **35**, 125 (2010).
[43]I. Mirebeau and G. Parette, Phys. Rev. B **82**, 104203 (2010).